Magnetoresistance enhancement in epitaxial magnetite films grown on vicinal substrates

S. K. Arora,* R. G. S. Sofin, and I. V. Shvets
SFI Nanoscience Laboratories, Physics Department, Trinity College Dublin, Dublin 2, Ireland
(Received 2 February 2005; revised manuscript received 1 July 2005; published 5 October 2005)

The magnetoresistance (MR) behavior of epitaxial magnetite Fe_3O_4 grown on low-vicinal (small miscut) and high-vicinal (large miscut) MgO substrates is compared. Magnetization measurements on Fe_3O_4 films on high-vicinal substrates showed reduced magnetic moment as compared with the films grown on low-vicinal MgO, which correlates well with the expected reduction in magnetic moment due to step edge induced additional antiphase boundaries (APBs) with out-of-plane shift vectors. The MR is significantly higher (12.3% at 2 T) for a 45 nm Fe_3O_4 film on high-vicinal substrate than that observed (7.2% at 2 T) for a film on low-vicinal substrate. A strong anisotropy in the MR is observed in correlation with the direction of atomic step edges. In addition to the increase in MR, the field dependency of the MR is also modified. The observed modification in the magnetotransport behavior of epitaxial Fe_3O_4 films is attributed to an enhanced spin scattering arising due to the presence of atomic height steps that lead to the formation of a greater density of antiferromagnetically coupled APBs.

DOI: 10.1103/PhysRevB.72.134404 PACS number(s): 75.47.−m, 72.25.−b, 75.50.Bb, 85.75.−d

INTRODUCTION

Recently, there has been a considerable amount of activity in the area of spin-dependent transport studies in magnetic nanostructures. The interest is driven by intriguing fundamental physics issues involved and the technological potential of such materials for spin electronic devices.[1,2] Among others, the simplest devices are spin valves and magnetic tunnel junctions, which are realized by separating two ferromagnetic electrodes by a normal metal or an insulating barrier, respectively.[3,4] Half metallic ferromagnetic (HMFM) materials possess 100% spin polarization and are expected to play an important role in spin-electronic devices. Some examples of half metallic ferromagnetic materials are: rare earth doped manganites, double perovskites, CrO_2, magnetite (Fe_3O_4), several Heusler alloys, etc.[5–7] Consequently, there are several reports on investigation of tunnel junction and spin valve devices made from these materials.[8–10] Alternative methods for growing biepitaxial junctions on step edges, bicrystals, and patterned surface have been utilized to attain better low-field magnetoresistance (MR) response.[11–13] An understanding of the mechanisms which govern the MR in these systems is complicated since they depend on many factors such as magnetic impurities, structural disorder, band structure, interfacial roughness, etc.[14,15]

Magnetite (Fe_3O_4) is an important half metallic ferromagnet with a high Curie temperature (T_c=858 K).[16] Because of its small lattice mismatch (−0.34%) with MgO, epitaxial growth of Fe_3O_4 thin films can be readily achieved on these substrates using a variety of deposition techniques.[17–23] The epitaxial growth of Fe_3O_4 on MgO suffers from the formation of antiphase boundaries (APBs), which are formed as a natural growth defect due to differences in the translational and rotational symmetry between Fe_3O_4 and MgO.[18,20,23]

The presence of APBs in epitaxial Fe_3O_4 films introduces local structural modifications and alters the magnetic interactions at the boundary making them predominantly antiferromagnetic.[24] This strongly affects the magnetic and electronic properties of the epitaxial Fe_3O_4 films. Because of the presence of APBs magnetization shows an anomalous behavior and it is difficult to saturate the films even with strong magnetic fields of up to several T, although the anisotropy field is only ~300 Oe for bulk Fe_3O_4.[18] Ultrathin Fe_3O_4 films (below 5 nm) exhibit super-paramagnetic behavior.[20] The MR behavior of magnetite thin films has been widely studied in films on different substrates such as MgO and $MgAl_2O_4$.[21,25–27] Compared to bulk magnetite, epitaxial Fe_3O_4 films show a greater MR, which is difficult to saturate even in strong magnetic fields. So far, the magnitude of MR observed in epitaxial films has not exceeded 8% for a magnetic field strength of 2 T. The unusual MR behavior of Fe_3O_4 films is attributed to the presence of APBs, and a spin valve mechanism was proposed by Eerenstein *et al.*[25] They have modeled the observed MR across the APBs employing a hopping conductivity model in which the spin-polarized transport occurs across the antiferromagnetic interface between two ferromagnetic chains. This model predicts a large MR effect across a single boundary. However, due to the random network of APBs obtained in Fe_3O_4/MgO heteroepitaxy, this effect is greatly smeared and it is not possible to obtain any quantitative information.

In this study we have employed a new approach, which allows for a selective extraction of the contribution of the antiphase boundaries from the total MR. In our study the MgO substrate has a miscut with respect to a low-index plane (100). In this case the islands of Fe_3O_4 forming at different atomic terraces nucleate independently from each other. Consequently, as the nucleation islands grow there is a significant chance that antiphase boundaries are formed along the step edges of the atomic terraces. This provides a unique way to engineer the APB density and their orientation in epitaxial magnetite films through the control of the miscut angle of the substrate. As the density of the APBs aligned along the step edges is greater than in the perpendicular direction, one expects to find a difference in the MR for current driven along and perpendicular to the direction of the step edges. It is important to emphasize that in the case of the film

grown on the MgO (100) substrate the crystallographic anisotropy makes no contribution to the measurements. Indeed, the two orthogonal directions on the (100) surface of a cubic crystal always correspond to equivalent crystallographic directions [e.g., (110) and (1–10)). Consequently, we decided to perform experiments on the MgO (100) substrate. In this study we measure the MR of Fe_3O_4 thin films for different substrate miscut angles and compare the results of MR along and perpendicular to the step edge direction.

We should point out that there has been some effort to improve the MR properties of magnetite films by utilizing bicrystal substrates[28] and microscopic step edge array on surfaces patterned by means of lithography.[29,30] The authors observed an enhancement in the MR that was not high in the low fields and was due to the spin-dependent electron transport across the magnetic clusters formed at the step edges. The studies[28–30] were not concerned with the APBs and indeed in the case of $Fe_3O_4/MgAl_2O_4$ the APBs are not formed as the film and substrate have the same kind of symmetry.

EXPERIMENTAL

Fe_3O_4 thin films used in the present study have been grown on (100) oriented MgO single crystal substrates using an oxygen plasma assisted molecular beam epitaxy (MBE) (DCA MBE M600, Finland) with a base pressure 5×10^{-10} Torr. We used two kinds of MgO (100) substrates: the first ones are low-vicinal (100) oriented single crystal substrates with a nominal miscut ±0.5° along an arbitrary direction and the other set of substrates had a 2° miscut on (100) oriented substrate along ⟨011⟩ direction within the accuracy of ±0.1°. The substrates were chemically cleaned prior to their insertion into the growth chamber and then cleaned *in situ* at 600 °C in UHV for 1 h followed by annealing in 1×10^{-5} Torr oxygen for 6 h duration. Growth of the Fe_3O_4 films has been carried out by means of electron beam evaporation of pure metallic Fe (99.999%) in presence of free oxygen radicals generated by the ECR (Electron Cyclotron Resonance) plasma source (OSPrey Plasma Source, Oxford Scientific, UK). The plasma source was operated at 80 W in an oxygen atmosphere of 1×10^{-5} Torr. Substrate temperature during growth was 250 °C. Details of the growth procedure are given elsewhere.[31] Reflection high-energy electron diffraction (RHEED) was employed to confirm the epitaxial growth and establish the growth mode. The presence of the RHEED intensity oscillations confirms that the films grow in a layer-by-layer mode (0.3 Å/s).

For electrical resistivity and magnetoresistance measurements a standard dc-four probe technique has been employed. The sample is mounted on a copper block fitted onto a cold finger of the closed cycle refrigerator. Temperature of the sample stage is monitored using a GaAlAs thermometer and controlled within ±0.05 K. For magnetotransport measurements, the cold finger is inserted into a variable field permanent magnet (Multimag, Magnetic Solutions, Ltd., Ireland). Using this magnet, it was possible to vary the strength (maximum field of 2 T) and orientation of the magnetic field in a desired direction. The magnetoresistance results reported here are obtained by keeping the direction of magnetic field and current parallel to each other unless otherwise stated. The MR is defined as $\mathrm{MR}\% = [R(H) - R(0)/R(0)]^* 100$, where $R(H)$ and $R(0)$ are the resistances of the sample with and without field, respectively. To determine the magnetoresistance anisotropy, the measurements have been carried out by passing current in two directions, which are orthogonal to each other, i.e., along and perpendicular to the direction of miscut (MC).

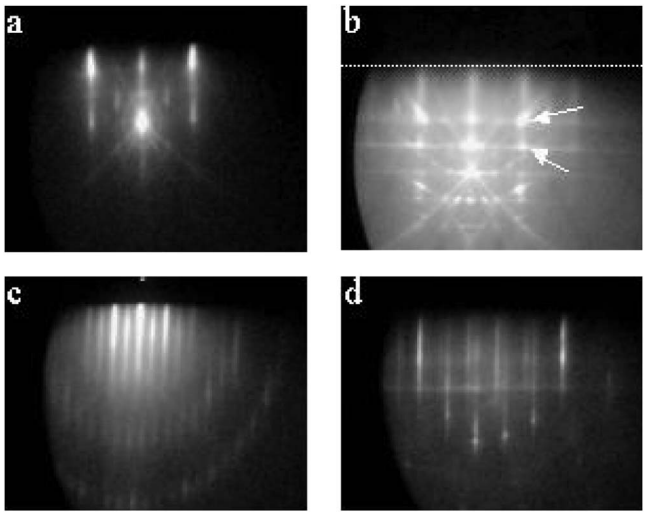

FIG. 1. RHEED images of high-vicinal MgO (100) substrate after the UHV heat treatment measured in [011] azimuths at room temperature with an incident electron beam direction (a) along and (b) perpendicular to the step edges direction, respectively. (c) and (d) are the RHEED images after the growth of 45 nm Fe_3O_4 film with an incident electron beam along and perpendicular to the step edges, respectively. Variations in streak separation are due to small changes in incidence angle of the electron beam for different azimuths. The dashed line in image (b) represents the shadow edge.

The miscut of the samples has been measured using the high-resolution x-ray diffraction (HRXRD) technique. To determine the miscut of the sample, the ω-rocking curves for (200) Bragg reflection of the substrate are measured at several azimuths. From the variation in incidence angle required to achieve the Bragg condition with the sample azimuth and fitting it using a sine function we determine the amplitude and direction of miscut.

RESULTS AND DISCUSSIONS

In the present study we provide comparative results on two 45 nm thick Fe_3O_4 films grown on low- and high-vicinal MgO (100) substrates, hereafter referred to as samples 1 and 2, respectively. Low- and high-vicinal samples had a miscut of 0.5° and 2.0°, respectively, along the ⟨011⟩ direction. In Figure 1 we show the RHEED images of the high-vicinal MgO (100) substrate recorded at room temperature after the UHV heat treatment [Figs. 1(a) and 1(b)]. These images were recorded in ⟨011⟩ directions. Small changes observed in the separation of vertical streaks are due to variations in incidence angle of the electron beam for different azimuths.

Figures 1(a) and 1(b) correspond to the case when electron beam is incident parallel or perpendicular to the step edge directions, respectively. For the case when the electron beam is incident along the step edges, the vertical lattice rods and sharp Kikuchi lines are observed. Sharp horizontal Kikuchi lines are observed only when the direction of incident electron beam is perpendicular to the step edges, which represents increased inelastic scattering due to the presence of atomic steps. These horizontal Kikuchi lines were found to have a tilt with respect to the shadow edge and were used to determine the average miscut angle of the substrate, which comes out to be 2.05°. We also checked the surface tilt from the position of the two diffracted spots marked with arrows in Fig. 1(b) with arrows using the following relation[32]:

$$\theta_c = \frac{\langle \theta_e \rangle}{2\pi/sd - 1}, \tag{1}$$

where $\langle \theta_e \rangle$ represent the average exit angle of the two diffraction spots, d is the planer spacing, and s denotes the spot separation in reciprocal lattice units. This gives a miscut angle of 2.1°. In Figs. 1(c) and 1(d) we show the RHEED pattern recorded after the growth of 45-nm Fe_3O_4 film on high-vicinal MgO(100) substrate. Additional streaks corresponding to Fe_3O_4 are situated in the middle of the MgO streaks. Other features are quite similar to those of the substrate for the case when the electron beam is incident along the step edges. For the incident beam direction perpendicular to the step edges there are additional features observed, and there are slashes alongside the vertical rods due to the additional periodicity arising from the terrace width. The average terrace width determined from the separation between the slashes and the diffraction streaks for the film is 5.69 (±0.5 nm) nm. The average miscut for sample 1 was found to be 0.5° within the accuracy of RHEED measurements. However, due to the larger terrace width of 24.05 nm for this sample, the additional slashes corresponding to the terraces were not observed. Instead, a broadening of streaks was noted. The estimated values of average miscut angles for both the samples were in good agreement with the results obtained through HRXRD measurements. HRXRD results showed that the average miscut angle for the substrate and the film after the growth were the same.

Figure 2 shows the ω-2θ rocking curves measured at room temperature for (200) and (400) Bragg reflections of the substrate and thin film respectively for samples 1 and 2. The horizontal axis in the figure is shown with reference to the Bragg angle for symmetric (200) reflection of MgO substrate. The curves are shifted along the vertical axis for clarity. From the separation between the film and substrate Bragg peaks we determine the out-of-plane lattice constant. For both the samples it is found to be 0.8372 nm. The full width at half maximum (FWHM) for the thin film peak is found to be 0.065 and 0.077 degrees for samples 1 and 2, respectively. Larger FWHM of the thin film peak for sample 2 represents additional scattering contribution arising from the presence of step edges. The in-plane lattice parameters of the films were determined from the asymmetric (622/311) Bragg reflections (not shown). We find that the in-plane lattice constant of Fe_3O_4 thin film (0.84236 nm) is twice that of the MgO substrate (0.4213 nm). Weak shoulder observed near the substrate peak for the ω-2θ rocking is Keissing fringe indicating a sharp interface between film and substrate. From the *in situ* RHEED and *ex situ* HRXRD characterization, we infer that the films grow pseudomorphically and maintain one-to-one registry with the MgO substrate. The unit cell volume of the film is a good indication of the film stoichiometry and is consistent with bulk magnetite suggesting that the films are stoichiometric.

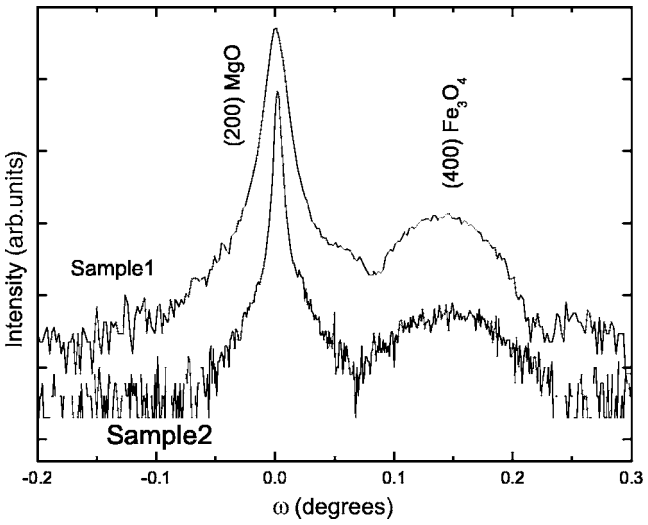

FIG. 2. The ω-2θ rocking curves of samples 1 and 2 measured relative to the (200) Bragg reflection of MgO.

Figure 3 shows the in-plane hysteresis loops measured at room temperature for both samples. Magnetization (M) values attained for samples 1 and 2 at 1 T field were found to be 468 and 445 emu/cm^3. These values are smaller than the saturation magnetization value of bulk Fe_3O_4 (480 emu/cm^3). It was not possible to saturate both the samples with the maximum available field strength of 1 T with the measurement set up. Observation of reduced magnetization and finite slope seen at higher fields is indicative of the presence of areas with frustrated exchange. Observation of reduced M and inability to saturate epitaxial Fe_3O_4 films is attributed to the presence of APBs.[18,20] The reduction in M was found to increase with the miscut angle and we relate this to the presence of step edges which enable the formation of additional APBs.

In order to estimate the contribution of step edges induced APBs to the observed reduced magnetic moment, one needs to work out their probability of formation along a given step edge. These estimates rely on certain assumptions in relation to the mechanism of nucleation of magnetite on MgO. Before going into the analysis in detail, it could be helpful to remind the reader that the crystal structure of magnetite is based on the fcc oxygen sublattice, similar to the oxygen sublattice of MgO. In this sublattice some of the tetrahedral interstices (so-called A sites) and some of the octahedral interstices (so-called B sites) are occupied by the Fe^{2+} and Fe^{3+} ions. The (100) atomic planes containing A and B sites are positioned in alternation and are separated by 0.1049 nm. Thus, the separation between the planes containing the like

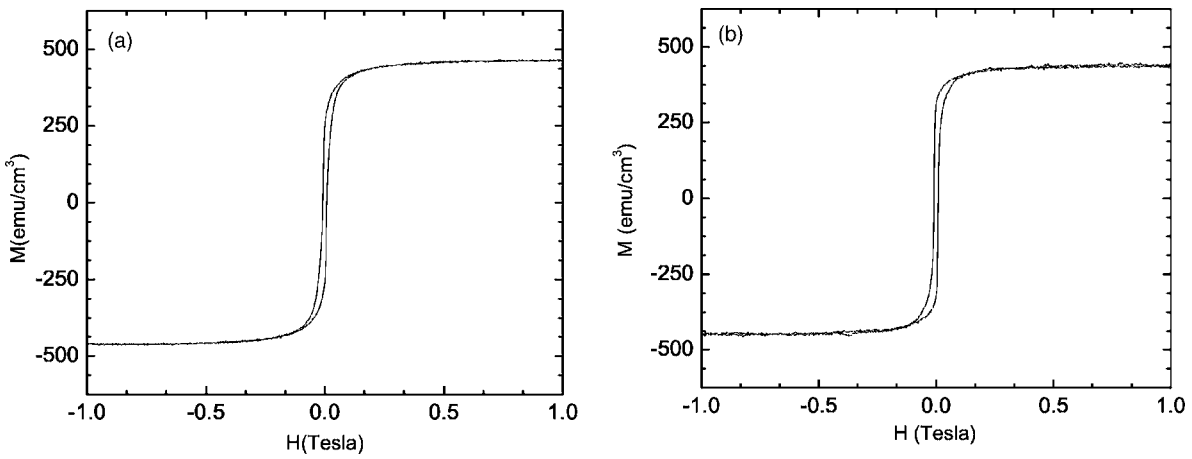

FIG. 3. Hysteresis loops of (a) sample 1 and (b) sample 2 measured at room temperature with an in-plane applied field.

sites (*A*-*A* or *B*-*B*), is 0.2099 nm. In the atomic planes containing *B* sites the Fe ions are positioned in rows along the ⟨110⟩ directions. The separation between the ions within the rows is 0.3 nm and the separation between the rows is 0.6 nm.

The key assumption in calculating the probability of APB formation is nucleation mechanism of magnetite. For example, if the nucleation on one of the two terraces separated by step edge starts at the atomic plane of *A* sites, and the nucleation on the other one starts at the atomic plane of *B* sites, then ABP is formed with certainty. This is clear because in the structure of magnetite, atomic planes separated by 0.2099 nm are planes of like interstices. Yet the body of experimental evidence coming from, e.g., the scanning tunneling microscopy (STM) studies, suggests that there is a large energy difference between the surfaces of *A*- and *B*-site terminations. Usually the *B*-site terminated surfaces are observed.[33,34] The type of surface termination is sensitive to the sample preparation conditions. Regardless of any preparation procedure, the two terminations are virtually never observed simultaneously on the same surface. Most of the STM data have been obtained on single crystals of magnetite, and not on Fe_3O_4/MgO films. Still, the data suggest that the likelihood of nucleation by *A*- and *B*-site planes simultaneously can be discounted. Let us first consider the case of nucleation by *B* sites that is preferred by the STM studies. Across a monoatomic step on the (100) surface of magnetite there are 32 possible combinations of positioning the nucleation islands on two neighboring terraces of MgO. To see if they result in the formation of the APB, we need to compare the positions of atoms in the third Fe atomic layer on the lower terraces with the positions of the atoms of the first Fe layer on the upper terrace. Of the 32 possible combinations, 16 have the nucleation rows of *B* sites on the upper terrace parallel to the ones on the lower terrace. All 16 combinations result in the formation of APBs. The remaining 16 combinations have the rows on the upper plane perpendicular to the rows on the lower plane. Of these 16 combinations, 8 result in the formation of the APBs and the remaining 8 do not. Therefore, there is 75% chance of forming an APB along the step edge if the nucleation starts at the *B* sites. Considering the second case when the nucleation starts at the *A* sites, it is possible to have 64 combinations, out of which only 8 combinations do not form APBs. So the total chance of forming APBs in this case will be 87.5%. Whether the magnetite nucleates at *A* or *B* sites, or even if there is nucleation at both sites simultaneously, one could see that there is a very high chance of formation of APBs along the step edge.

For 0.5° and 2° miscut along the ⟨011⟩ direction of MgO ⟨100⟩ substrate the average terrace width is 24.05 and 5.96 nm, respectively. This corresponds to a step density of 4.9×10^5 and 1.6×10^6 cm^{-1}, resepectively, for samples 1 and 2. By considering this number density of APB and a width of 0.42 nm (by assuming that at the APB one bond from each side of the boundary contributes to the frustrated exchange) we estimate the area of the frustrated volume to be ~1.52 and 5.6% for samples 1 and 2, respectively. However, we observe a 2.28 and 7% reduction in magnetic moment for samples 1 and 2, respectively. The additional enhancement of area with frustrated magnetic moment is possibly due to the presence of natural shifted APBs at the terraces. From RHEED and magnetization results we infer that the films grown on low- and high-vicinal substrates possess APBs formed due to the step edges. Now, we turn our attention to the magnetoresistance results obtained on these samples.

First, we present the magnetoresistance results obtained from sample 1 (45 nm thick Fe_3O_4 film grown on low-vicinal MgO (100) substrate having a miscut of 0.5° along the ⟨011⟩ direction). Sample 1 exhibited a Verwey transition at 108 K and its magnetoresistance was studied as a function of temperature. Figure 4(a) shows the magnetoresistance measured in the ⟨001⟩ direction at 150 and 108 K as a function of magnetic field applied in the film plane. The MR is found to increase with decreasing temperature and is substantially higher near the Verwey transition temperature (T_v). Figure 4(b) shows the MR results obtained for this sample measured at the Verwey transition (108 K) in the ⟨010⟩ direction, along and perpendicular to the step edges. The MR at 2 T field measured across the step edges is found to be 7.54%, which is 2.69 and 1.93 % higher than the MR along the ⟨010⟩ and step-edge directions, respectively. The enhancement in the MR is more prominent at lower temperatures particularly in the Verwey transition region. Some difference between the curves measured along the ⟨100⟩ and the

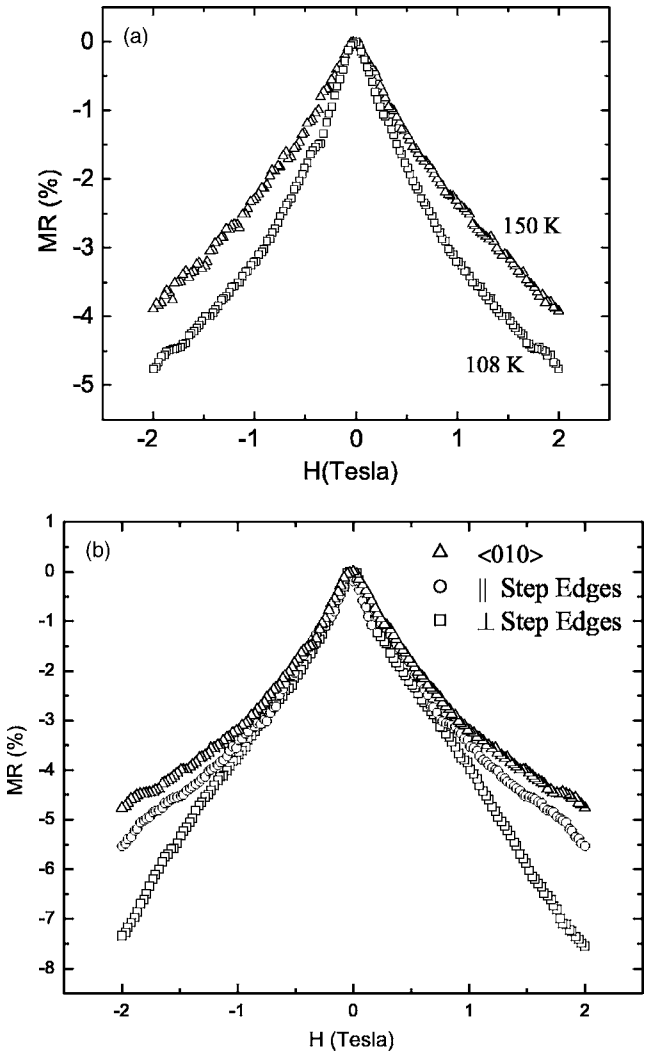

FIG. 4. (a) Magnetoresistance of sample 1 at 150 and 108 K with the magnetic field applied in the film plane. (b) Magnetoresistance measured at the Verwey transition temperature (108 K) in the ⟨010⟩, along and perpendicular to the step-edge directions.

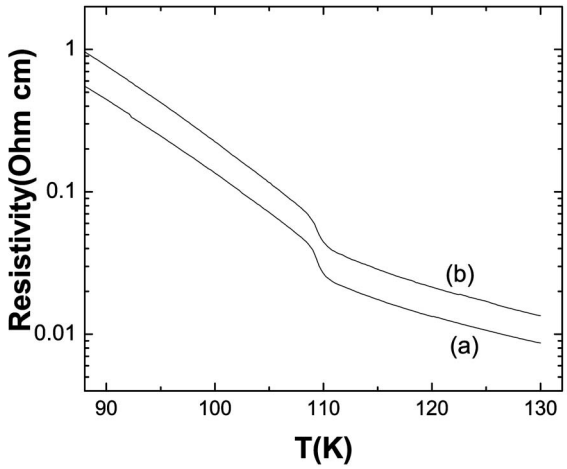

FIG. 5. Resistivity as a function of temperature measured (a) along and (b) perpendicular to the step edges for sample 2 [45-nm-thick Fe_3O_4 film on MgO (100) substrate with 2° miscut along the ⟨011⟩ direction].

miscut directions is expected. Indeed, these two directions are crystallographically inequivalent as the miscut direction is effectively along the ⟨110⟩ direction. However, two directions, along and perpendicular to the miscut, are crystallographically equivalent, consequently no anisotropy in the transport properties between these two directions is expected. We suggest that the anisotropy results from the preferential alignment of APBs along the step edges as explained in the introduction. Thus, formed APBs enhance the spin-dependent scattering and influence the MR properties.

Our results on sample 1 demonstrate that it is possible to control the MR properties of magnetite thin films and introduce MR anisotropy provided the density and orientation of APBs is controlled. In Fig. 5 we show the temperature variation of resistivity (ρ) measured along and perpendicular to the step edges for sample 2 (45-nm-thick Fe_3O_4 film grown on high-vicinal MgO (100) substrate having a miscut of 2 degrees along the ⟨011⟩ direction). The Verwey temperature for both directions is found to be 109.8 K. The resistivity across the step edges is about 2 times greater than the resistivity along the step edges (at 130 K ρ was found to be 8.6 and 13.6 mΩ cm along and across the step edges, respectively). The resistivity versus temperature dependency for the Fe_3O_4 films shows an activated behavior with an activation energy of ~30 meV above the Verwey transition temperature for both directions. Below the Verwey transition temperature the activation energies are found to be 56 and 61 meV along and across the step edges respectively. The resistivity anisotropy remains persistent throughout the whole temperature range. The enhancement in resistivity across the step edges is due to a significant increase in the density of APBs formed at the step edges that produces an additional scattering of charge carriers traversing across the step edges. This substantially reduces the mobility of charge carriers across the step edges and an anisotropic mobility with respect to the relative direction of current and step edges is observed. The resitivity for sample 1 showed similar behavior. At 130 K the resistivity was found to be 4.68 and 5.09 mΩ cm when measured along and across the step edges. The lower resistivity obtained for sample 1 as compared with sample 2 demonstrates that the step edges facilitate the formation of APBs. This further supports our conclusion based on magnetization reduction. Conduction properties of Fe_3O_4 thin films possessing APBs have been studied by Eerenstein *et al.*[25] within the framework of a one-dimensional hopping model. The conductivity predicted by this model is proportional to t^2, where t ($t=t_0 \cos \varphi_{nn}$) is the transfer integral. According to this model the presence of local structural and spin disorder at the APB reduces the transfer integral. This suggests that in the case of vicinal substrate where the APBs are formed predominantly at the step edges, one expects a reduction in the conductivity along the MC direction, which is in line with the experimental observations.

Magnetoresistance of sample 2 was studied as a function of temperature along and across the direction of the step edges. Figure 6 shows the representative MR curves for sample 2 measured along and across the step edges at 130,

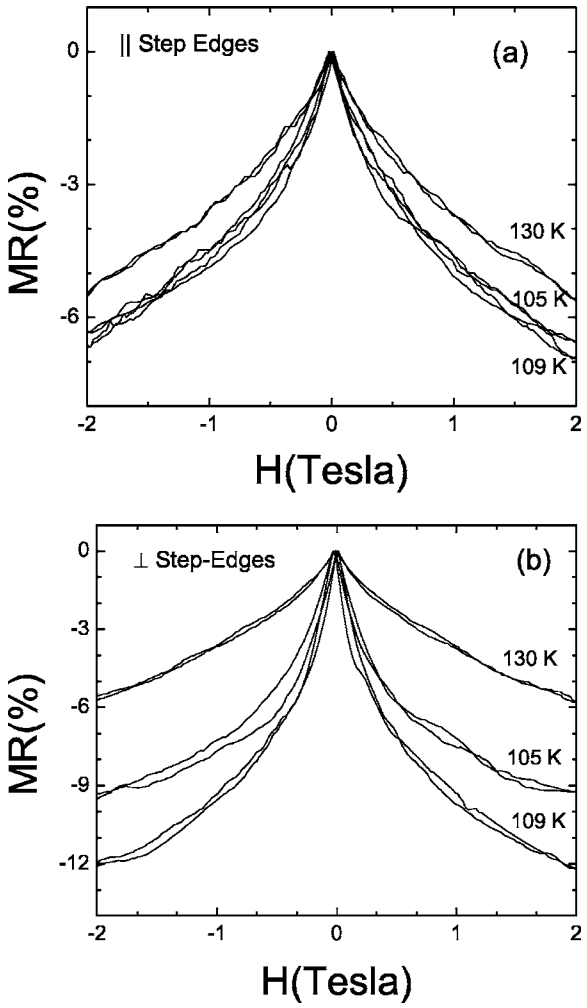

FIG. 6. Magnetoresistance as a function of applied in-plane magnetic field for sample 2, measured at different temperatures (a) along and (b) perpendicular to the direction of step edges. The direction of current and magnetic field are parallel to each other.

109, and 105 K, respectively. The MR is found to be strongly anisotropic with respect to the direction of the step edges: the MR across the step edges is significantly higher than along the step edge direction. The magnitude of MR for both directions is found to increase with a decrease in temperature and peaks at the Verwey transition temperature (109 K). A further decrease in the temperature leads to a lowering of the MR for both directions. The maximum value of MR is observed in the Verwey transition region, which is 12.2% at 2 T field and 9.7% at 1 T field. These values of MR are 5.4 and 4.4 % higher than the corresponding values observed along the step edges. The MR at 1 T field for sample 2 is found to be 4.7% higher than that of the low miscut sample. The difference in MR along and across the step edges is significantly higher only at the low temperatures mainly in the vicinity of the Verwey transition. The remarkable result is that there is a significant enhancement in the low field MR. The MR shows a steep rise up to a field of 0.7 T. For higher magnetic fields (>0.7 T) there is a crossover to shallower field dependence. However, the field dependence of MR along the step edges did not show this

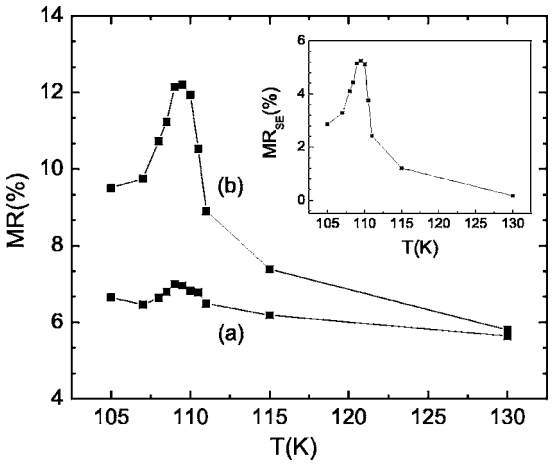

FIG. 7. Temperature dependence of the MR (a) along and (b) perpendicular to the step edges for sample 2. The inset shows the difference in MR observed for both the directions representing the step edge induced contribution to MR.

changeover. In Fig. 7, we show the temperature variation of the MR (2 T) measured along and across the step edges. The anisotropy in MR, $MR_{SE}=MR_{\perp}-MR_{\parallel}$, represents the contribution arising due to the step edges and is shown in the inset of Fig. 7. The anisotropy in MR is observed only below 150 K and peaks at the Verwey transition.

The observed values of MR are higher than any of the previously reported MR values for epitaxial magnetite films.[25–30] Previous efforts by Ziese *et al.*[29,30] to enhance the MR of epitaxial Fe_3O_4 films grown on patterned MgO and $MgAl_2O_4$ substrates having step edge array (80–120 nm step height and 10–20 μm wide stripes) have not yielded substantial MR increase. They found that the anisotropy in MR with reference to the step-edge direction was not large (1.8% at 3 T, 80 K) for the case of films grown on patterned MgO substrates, whereas they obtained relatively larger MR anisotropy for films grown on patterned $MgAl_2O_4$ (5% at 3 T, 105 K). They attribute the results on patterned MgO to the presence of larger density of APBs within the stripe. For films grown on patterned $MgAl_2O_4$, the disorder at step edges enhances the spin scattering leading to a larger anisotropy in MR, since the effect due to step edges is not smeared by the APBs. Recently, Bollero *et al.*[28] have reported that due to the presence of APBs within the film, Fe_3O_4 films grown on bicrystal MgO(100) substrate having a 28° grain boundary did not yield any enhancement in MR across the grain boundary. In our case, due to the preferential alignment of step edges along the direction perpendicular to the miscut, APBs are formed due to the presence of atomic height steps (0.21 nm) on MgO substrate (as described in detail in the preceding discussion). The terrace width (24.05 and 5.96 nm for 0.5° and 2° miscut, respectively) is quite small in comparison to the width of step edge array used by Ziese *et al.*[29,30]

The MR behavior of epitaxial magnetite thin films containing APBs has been analyzed by Eerenstein *et al.*[25] and Zeise and Blythe[26] within one-dimensional models. Concerning the MR of the Fe_3O_4 films on vicinal substrates, we noticed that contrary to the prediction of the models, the field

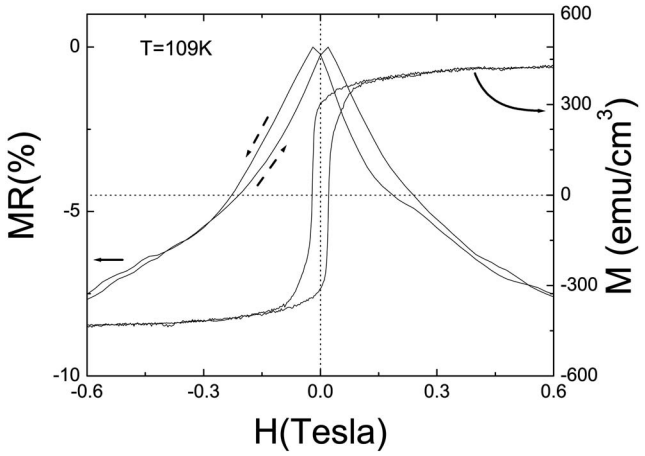

FIG. 8. Magnetoresistance as a function of applied magnetic field for sample 2 measured across the step edges at 109 K along with the magnetization loop at the same temperature. Dashed and solid arrows indicate the direction of field increase and the scales corresponding to the curves, respectively.

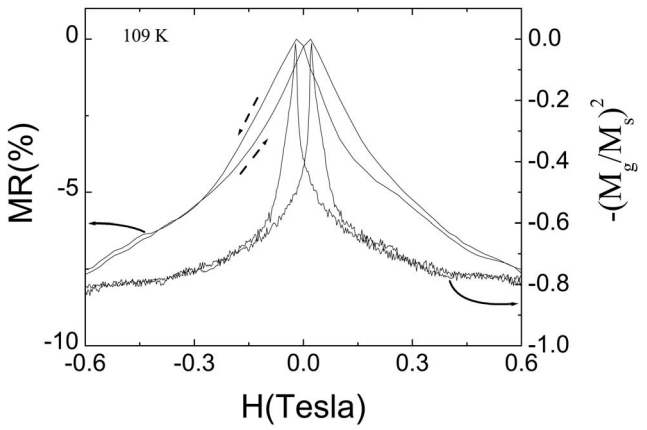

FIG. 9. Magnetoresistance of sample 2 along with the bulk magnetization normalized to the saturation magnetization $-(M_g/M_s)^2$, as a function of applied magnetic field measured across the step edges at 109 K. Dashed and solid arrows indicate the direction of field increase and the scales corresponding to the curves, respectively.

dependence of MR deviates from a linear behavior below a certain temperature (130 K). The above models assume quite a simplified spin structure of APB whereas the spin structure could be more complex. The spin-dependent scattering across the APB will be strongly influenced by spin structure and the strain fields associated with it. Furthermore, to explain the temperature and field dependence of MR, variations in the mismatch strain with the temperature and presence of the Verwey transition also need to be considered. If the additional MR induced by the step edges arises due to the spin polarized tunneling (SPT) across the APBs, one expects the MR to scale with the spin polarization P. The dependence of spin polarization on magnetization (M) is complex but we use Julliere's model[35] within the first approximation ($P \propto M$), this predicts the MR as

$$\mathrm{MR} = P^2/(1+P^2). \tag{2}$$

From Eq. (2), one would expect the MR to follow the relation

$$\mathrm{MR} \propto -(M_g/M_s)^2, \tag{3}$$

where M_g and M_s are the global magnetization and saturation magnetization, respectively. This model is quite successful in explaining the MR behavior of devices made of bicrystal or grain boundary junctions.[12,30,36] In Fig. 8 we plot the magnetization and MR in low field across the step edges. The MR peaks at the coercivity fields of the film (H_c=205 Oe). A similar correlation with the coercive field was noted throughout the temperature range. To check the validity of the model yielding the dependence (3), we plot MR against the squared magnetization normalized to the saturation magnetization $-(M_g/M_s)^2$ (Fig. 9). Only a small fraction of the observed low field MR can be explained on the basis of relation (3). The observation of two-step transition from a sharp low field MR to a gradual high field MR (the crossover field being much greater than the coercive field) for our case cannot be explained within the simplified picture of Julliere's model.[35] This model assumes that the extent of SPT depends on barrier conductance and relative orientation of magnetization directions of uniformly magnetized spin systems on each side of the boundary, which are magnetically decoupled. In our case, the situation is more complicated due to the reason that the magnetization vectors across an APB are closely related. Moreover, tunnelling probability could be affected from the variations in local magnetization within the domain, atomic arrangement and spin configuration of the APBs, terrace width, etc. Although, our observations are not in agreement with the relation (3), the MR contribution arising from SPT cannot be completely ruled out. In order to explain the MR in the films we consider spin-dependent scattering at the antiphase boundaries. Such scattering results from the spin-spin interaction. The second mechanism of the scattering could be that the lattice deformation takes place at the APB resulting from the magnetostriction. The magnetostriction is altered by the external magnetic field that changes the scattering. Needless to say, the scattering at the APBs is additional to the other spin-dependent scattering taking place within the grains and thus outside the scope of this paper. The misaligned direction of spins at the APB leading to the spin scattering is a result of two factors: the frustrated exchange across the APB and the interaction with the domains adjacent to the APB. With increasing magnetic field, the magnetic domains adjacent to the APBs pull against the frustrated exchange interaction and reduce the magnetic inhomogeneity at the APB and consequently the scattering induced by it. This model explains the observations in the higher magnetic field (above 1 T) whereby the MR increases with the field and yet the magnetization is virtually saturated. Indeed the volume of the region with frustrated exchange at the boundaries is very small by comparison with the overall volume of the sample. Therefore, the more collinear alignment of the spins at the APB has no significant effect on the M_g. Still, these APBs with increased co-linearity of the spins become less effective in scattering electrons. The model is schematically presented in Fig. 10. For simplicity, only one

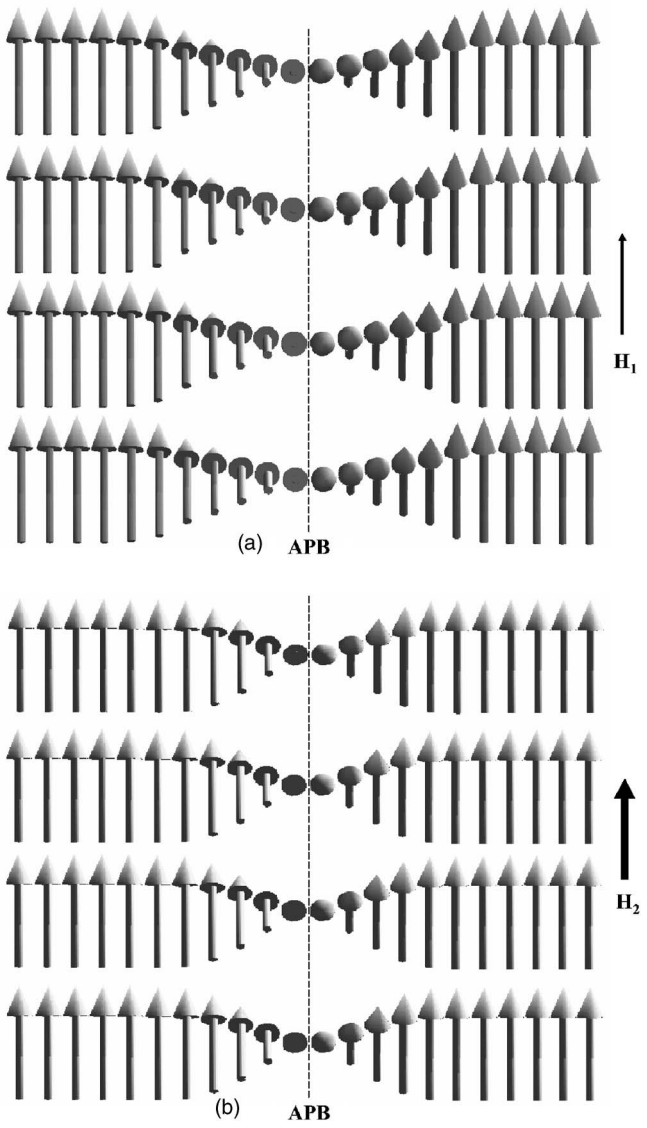

FIG. 10. Spin structures for one of the magnetic sublattice of magnetite across an antiphase boundary for (a) weak and (b) strong magnetic fields, respectively, showing the variations in domain wall widths with an applied magnetic field.

of the magnetic sublattices of magnetite is shown. The Figs. 10(a) and 10(b) schematically show the situation with smaller and greater field values, respectively. Figure 10(b) shows that the width of the area with misaligned spins is reduced when a stronger magnetic field is applied. In a recent investigation we have shown that the extent of exchange coupling induced by the APBs depends on the thermomagnetic history of the sample.[37] Our results also suggest that the APBs are nonstoichiometric with defects expected at both cationic and anionic sublattices.[38]

The above mechanism is based on the same concept of magnetoresistance caused by spin-dependent scattering as applied in spin valves. An alternative mechanism of the anisotropy of MR can be constructed in particular with the view to explain the temperature dependence of the magnetoresistance. In our experiments the MR increases substantially in the vicinity of the Verwey transition and the MR anisotropy develops at the same time. The increase in MR at the Verwey transition is not unusual and is reported by several other researchers in thin films and bulk single crystal of magnetite.[26,27,39] To explain the presence of MR peak in the vicinity of Verwey transition, Girdin and co-workers[39] used the established facts regarding the transport in Fe_3O_4 and thermodynamic arguments related to the Verwey transition. Tracing the discontinuous changes in enthalpy and entropy with resistivity, they proposed that the jump in MR can be described as $\phi^* = \Delta MH/k_B \delta T_{1/2}$, where ΔM is the change in magnetization across T_v and $\delta T_{1/2}$ is the full-width at half maximum of the MR peak at T_v. They correlated the MR peak amplitude with the discontinuous changes in magnetization (0.1% decrease) and the width of transition. Small decrease in magnetization could be related to the partial condensation of optical phonon modes. In a recent report, Ogale *et al.*[27] have reported the presence and absence of MR peak in magnetite thin films of (100) and (111) orientations, respectively. Their data emphasize the role of strong electron-phonon coupling and polaronic correlation effects in context of the carrier transport in Fe_3O_4. These observations explain the gross feature of temperature dependence in our case, but not the difference in the magnitude of MR for two directions reported here. As discussed below, the observed results can be explained by the anisotropy in magnetoelastic properties of the films induced by the presence of APBs and the subsequent modifications to the polaronic states.

For a start we should point out that the Verwey transition in our films is of the first order as indeed expected for stoichiometric magnetite. This is confirmed by the presence of the hysteresis in the temperature dependencies of magnetization and resistivity. In our recent study[40] we have shown that the presence of APBs affects the elastic property of the films and enables them to maintain a fully strained state up to thickness much greater than those estimated from the mismatch strain, as there is compressive strain at the domain boundaries. Because of the highly directional nature of step edge induced APBs in the films grown on vicinal substrates the elastic properties of the film will be anisotropic. This suggests that the magnetoelastic response of these films will depend on the relative orientation of the magnetic field and step edges. Therefore, the magnetostriction anisotropy will cause distinctly different modifications of internal stress and correspondingly the phonon spectra for the two directions: along and perpendicular to the step edges. In addition to anisotropic elastic properties, the structural disorder associated with the APB modifies the cationic coordination and affects the nearest- and next-nearest-neighbor Coulomb interactions energies that are responsible for the short- and long-range ordering of carriers.

Given the magnetoelastic coupling, the application of a magnetic field will affect the coupled phonon-magnon modes as well as the nearest- and next-nearest-neighbor interactions energies differently along the two directions. Consequently, this alters the electron-phonon coupling and broadens the polaronic bands in an anisotropic way that directly affects the formation of a charge ordered state. The polaronic hopping energy, which is proportional to the inverse square of the optical phonon frequency will be affected by the application of a magnetic field via coupled phonon-magnon

modes. Decrease in activation energy across the step edges in our case reflects the softening of magnon modes and correspondingly the phonon-magnon modes due to applied magnetic field. Moreover, the variations in mismatch strain due to differences in the thermal expansion coefficients of Fe_3O_4 and MgO and strain associated with the cubic-monoclinic structural phase transition at the Verwey temperature will also have an influence on the charge ordering process. In light of the above suggestions, the application of a magnetic field will suppress the formation of a charge ordered state across the step edges to a greater extent than along them leading to a larger amplitude of MR across the step edges. The above physical picture explains qualitatively the observed anisotropy in the MR peak magnitude, but the precise mechanism is not clear at this time.

In our study we have also noticed that the MR enhancement depends strongly on the way the substrate surface has been treated prior to the growth of the magnetite film. This subsequently determines the nature of the film microstructure as well as the nature and density of APBs that will strongly affect the MR properties. The detailed results will be reported later.

CONCLUSION

In summary, we have observed a strong anisotropy in the MR in close correlation with the direction of current and step edges in epitaxial Fe_3O_4 films grown on vicinal MgO (100) substrate. Magnetization measurements clearly demonstrate the formation of a greater number of antiferromagnetically coupled antiphase boundaries due to the presence of step edges present on a vicinal substrate. We describe two mechanisms for the observed difference in MR along two equivalent crystallographic directions on the surface. The first one is based on spin-dependent electron scattering along the APBs. The second mechanism suggests a difference in the reduction of magnetization values along and across the APBs resulting from the difference in magnetoelastic properties. The increase in the low field MR due to the step induced spin scattering in Fe_3O_4 films is an important result to realize future spin-electronics applications of magnetic nanostructures. We wish to point out that the differences in the values of MR reported for Fe_3O_4 films are linked to the microstructural properties and strongly depend on the miscut magnitude and direction. Antiphase boundaries are expected to form in various other spinel materials as well as numerous nonspinel films provided the substrate for the epitaxial film growth is chosen correctly. Therefore, we suggest that the observed increase in magnetoresistance is not necessarily limited to magnetite films only. It is likely that magnetoresistance of some other epitaxial films could be enhanced in the same way if the films are grown on vicinal substrates and the pattern of antiphase boundaries with preferential orientation is formed.

ACKNOWLEDGMENTS

The authors gratefully acknowledge the financial support from the Science Foundation Ireland to carry out the work under the Project No. 00/PI.1/C042.

*Electronic address: aroras@tcd.ie

[1] I. Zutic, J. Fabian, and S. Das Sarma, Rev. Mod. Phys. **76**, 323 (2004).
[2] M. Ziese, Rep. Prog. Phys. **65**, 143 (2002).
[3] G. A. Prinz, J. Magn. Magn. Mater. **200**, 57 (1999).
[4] R. Jansen, J. Phys. D **36**, R289 (2003).
[5] J. M. D. Coey, M. Viret, and S. von Molnar, Adv. Phys. **48**, 167 (1999).
[6] W. E. Pickett and D. J. Singh, Phys. Rev. B **53**, 1146 (1996).
[7] R. A. de Groot, F. M. Mueller, P. G. van Engen, and K. H. J. Buschow, Phys. Rev. Lett. **50**, 2024 (1983).
[8] A. Gupta, X. W. Li, and G. Xiao, Appl. Phys. Lett. **78**, 1894 (2001).
[9] M. H. Jo, N. D. Mathur, N. K. Todd, and M. G. Blamire, Phys. Rev. B **61**, R14905 (2000).
[10] K. S. Takahashi, A. Sawa, Y. Ishii, H. Akoh, M. Kawasaki, and Y. Tokura, Phys. Rev. B **67**, 094413 (2003).
[11] M. Ziese, G. Heydon, R. Hohne, P. Esquinazi, and J. Dienelt, Appl. Phys. Lett. **74**, 1481 (1999).
[12] M. Sussiau, F. Nguyen-Van-Dau, P. Galtier, and A. Schuhl, Appl. Phys. Lett. **69**, 857 (1996).
[13] Mandar Paranjape, J. Mitra, A. K. Raychaudhuri, N. K. Todd, N. D. Mathur, and M. G. Blamire, Phys. Rev. B **68**, 144409 (2003).
[14] E. Y. Tsymbal, O. N. Mryasov, and P. R. LeClair, J. Phys.: Condens. Matter **15**, R109 (2003).
[15] A. Fert, A. Barthelemy, J. Ben Youssef, J. P. Contour, V. Cros, J. M. De Teresa, A. Hamzic, J. M. George, G. Faini, J. Grollier, H. Jaffres, H. Le Gall, F. Montaigne, F. Pailloux, and F. Petroff, Mater. Sci. Eng., B **84**, 1 (2001).
[16] F. Walz, J. Phys.: Condens. Matter **14**, R285 (2002).
[17] D. M. Lind, S. D. Berry, G. Chern, H. Mathias, and L. R. Testardi, Phys. Rev. B **45**, 1838 (1992).
[18] D. T. Margulies, F. T. Parker, F. E. Spada, R. S. Goldman, J. Li, R. Sinclair, and A. E. Berkowitz, Phys. Rev. B **53**, 9175 (1996).
[19] P. A. A. van der Heijden, P. J. H. Bloemen, J. M. Metselaar, R. M. Wolf, J. M. Gaines, J. T. W. M. van Eemeren, P. J. van der Zaag, and W. J. M. de Jonge, Phys. Rev. B **55**, 11569 (1997).
[20] F. C. Voogt, T. T. M. Palstra, L. Niesen, O. C. Rogojanu, M. A. Janes, and T. Hibma, Phys. Rev. B **57**, R8107 (1998).
[21] X. W. Li, A. Gupta, Gang Xiao, and G. Q. Gong, J. Appl. Phys. **83**, 7049 (1998).
[22] Sangeeta Kale, S. M. Bhagat, S. E. Lofland, T. Scabarozi, S. B. Ogale, A. Orozco, S. R. Shinde, T. Venkatesan, B. Hannoyer, B. Mercey, and W. Prellier, Phys. Rev. B **64**, 205413 (2001).
[23] W. Eerenstein, T. T. M. Palstra, T. Hibma, and S. Celotto, Phys. Rev. B **68**, 014428 (2003).
[24] D. T. Margulies, F. T. Parker, M. L. Rudee, F. E. Spada, J. N. Chapman, R. A. Aitchison, and A. E. Berkowitz, Phys. Rev. Lett. **79**, 5162 (1997); W. Eerenstein, Ph.D. thesis, Univ. of Groningen, Groningen, The Netherlands, 2003.

[25] W. Eerenstein, T. T. M. Palstra, S. S. Saxena, and T. Hibma, Phys. Rev. Lett. **88**, 247204 (2002).
[26] M. Ziese and J. Blythe, J. Phys.: Condens. Matter **12**, 13 (2000).
[27] S. B. Ogale, K. Ghosh, R. P. Sharma, R. L. Greene, R. Ramesh, and T. Venkatesan, Phys. Rev. B **57**, 7823 (1998).
[28] A. Bollero, M. Ziese, P. Esquinazi, K. Dorr, and I. Monch, J. Magn. Magn. Mater. **290-291**, 1134 (2005).
[29] M. Ziese, R. Hohne, N. H. Hong, J. Dienelt, K. Zimmer, and P. Esquinazi, J. Magn. Magn. Mater. **242–245**, 450 (2002).
[30] M. Ziese, R. Hohne, H. C. Semmelhack, K. H. Han, P. Esquinazi, and K. Zimmer, J. Magn. Magn. Mater. **279**, 331 (2004).
[31] Y. Zhou, Xuesong Jin, and I. V. Shvets, J. Appl. Phys. **95**, 7357 (2004).
[32] W. Braun, *Applied RHEED: Reflection High Energy Electron Diffraction During Crystal Growth*, Springer Tracts in Modern Physics (Springer, Berlin, 1999), Vol. 154; H. Abe, M. Kanemura, T. Egawa, Y. Nabetani, T. Kato, and T. Matsumoto, J. Cryst. Growth **241/215**, 595 (2000).
[33] G. Mariotto, S. Murphy, and I. V. Shvets, Phys. Rev. B **66**, 245426 (2002).
[34] I. V. Shvets, G. Mariotto, K. Jordan, N. Berdunov, R. Kantor, and S. Murphy, Phys. Rev. B **70**, 155406 (2004).
[35] M. Julliere, Phys. Lett. **54A**, 225 (1975).
[36] J. E. Evetts, M. G. Blamire, N. D. Mathur, S. P. Isaac, B. S. Teo, L. F. Cohen, and L. Macmanus-Driscoll, Philos. Trans. R. Soc. London, Ser. A **356**, 1593 (1998).
[37] S. K. Arora, R. G. S. Sofin, A. Nolan, and I. V. Shvets, J. Magn. Magn. Mater. **286**, 463 (2005).
[38] Y. Zhou, X. Jin, and I. V. Shvets, J. Magn. Magn. Mater. **286**, 346 (2005).
[39] V. V. Gridin, G. R. Hearne, and J. M. Honig, Phys. Rev. B **53**, 15518 (1996).
[40] K. Balakrishnan, S. K. Arora, and I. V. Shvets, J. Phys.: Condens. Matter **16**, 5387 (2004).